Bimetallic Pt or Pd-based carbon supported nanoparticles are more stable than their monometallic counterparts for application in membraneless alkaline fuel cell anodes

Huong Doan, Thiago Morais, Nino Borchtchoukova, Yair Wijsboom, Ronit Sharabi, Marian Chatenet, Gennadi Finkelshtain

Bimetallic Pt or Pd-based carbon supported nanoparticles are more stable than their monometallic counterparts for application in membraneless Alkaline Fuel Cell anodes

Huong Doan [1#], Thiago Morais [1-2#], Nino Borchtchoukova [3], Yair Wijsboom [3], Ronit Sharabi [3], Marian Chatenet [1,*] and Gennadi Finkelshtain [3]

[1] *Univ. Grenoble Alpes, Univ. Savoie Mont Blanc, CNRS, Grenoble INP (Institute of Engineering and Management Univ. Grenoble Alpes), LEPMI, 38000 Grenoble, France*

[2] *University of São Paulo, Institute of Chemistry, São Carlos, State of São Paulo, Brazil*

[3] *GenCell Energy, Petach Tikva, Israel*

Co-first authors

* Corresponding author

marian.chatenet@grenoble-inp.fr

Abstract

Alkaline fuel cells (AFCs) are relevant for niche applications, but still require enhanced performance and lifetime. Active and durable hydrogen oxidation reaction (HOR) catalysts must be developed: linking their electrochemical surface area (ECSA) loss to their HOR activity and understanding whether the ECSA loss of carbon-supported platinum group metal-based (PGM/C) HOR catalysts is irreversible (nanoparticles dissolution, detachment, Ostwald ripening) or reversible is pivotal. Using identical-location transmission electron micrographs (IL-TEM) and ECSA characterizations by "CO-like" stripping undertaken pre and post accelerated stress tests (AST), the different degradation mechanisms undergone by monometallic (Pt/C and Pd/C) and

bimetallic catalysts (Pd-Pt/C and Pd-Ni/C) are unveiled. Monometallic PGM/C undergo extensive reversible poisoning and irreversible degradation upon operation at low potential, in contrast to bimetallic catalysts, which are less affected. Pd-Ni exhibits the smallest loss of $ECSA_{PGM}$ and HOR activity: it poorly catalyzes carbon corrosion and is hardly poisoned by "CO-like" species.

1. Introduction

Hydrogen-fed fuel-cells (FCs) are advanced zero-emission technologies that only emit water as the byproduct. Although proton-exchange membrane fuel cells (PEMFCs) are now nearly mature (PEMFC-powered vehicles are produced since 1999-2000 and several brands commercialize a PEMFC-EV today), their system's cost remains too high, notably due to the expensive and rare platinum group metal (PGM) catalysts they employ in non-negligible amounts. Switching from acid to alkaline fuel cells (AFCs), either with an anion-exchange membrane (AEM) or with a porous separator, would enable to lower the materials cost of the fuel cell, because reduced-PGM or non-PGM catalysts can be used without significant performance loss (e.g. Pd-Ni-based catalysts led to high and stable performance in laboratory-scale unit AEMFC).[1] While AEMFC is getting more attention, the membrane remains an issue, owing to its limited durability high-temperature operation and propensity to be poisoned by carbonate species forming upon contact with air, which affects the OH^- transport[2,3]. In contrast, membraneless AFCs do not have these limitations: the use of circulated 30-40% KOH electrolyte through the chemically-stable porous separator helps facilitating water and thermal management and makes the system more robust versus external (environmental) conditions, thereby improving its lifetime and efficiency in extreme conditions.[4] As a matter of fact, the membraneless AFC technology has been successfully demonstrated since the 1950s for projects such as the NASA Apollo program or a liquid-AFC-

powered automobile (Austin A40 hybrid city car); it nowadays continues to demonstrate some advantages over PEMFC, or even AEMFC, mostly because of lower carbon corrosion and minimal water management issues.[5,6] The literature also reports that the performance of non-PGM catalysts for oxygen reduction reaction (ORR) in alkaline media is enhanced *versus* acid media, these materials being less prone to peroxyle radical attack at high pH, because hydrogen peroxide is chemically unstable in alkaline environment; specifically, Ag-based and Co-based catalysts were successfully evaluated in both half-cell and full cell AEMFC long durability test.[7,8]

One big challenge of AFCs though, is the search for a suitable hydrogen oxidation reaction (HOR) catalyst that can minimize the overpotential of the reaction, usually larger in alkaline environment than in acidic one.[1,9,10] Unfortunately, there is still no ideal alkaline HOR catalyst at the moment: even the most performing ones, based on PGM, fail to demonstrate equivalent HOR activity in base than in acids. Using carbon-supported PGM catalysts (the standard in PEMFCs and mostly-commercialized FC catalysts) in alkaline even has drawbacks: their alkaline durability is indeed insufficient. This is not linked to their corrosion resistance (which is manifest in alkaline environments [11]), but instead lies in the fact that PGM nanoparticles assist the local carbon corrosion at their vicinity[12–15], by facilitating the oxidation of "CO-like species" that naturally form on carbon above 0.2 V *vs* RHE, leading to CO_2 and carbonates formation, and finally to the PGM nanoparticles detachment.[16–18] Among the monometallic PGM, Pt catalyzes this oxidation reaction vigorously and yields the highest electrochemical surface area (ECSA) loss by severe nanoparticles detachment from the carbon support.[16–19] It is clear that once Pt nanoparticles are disconnected/detached from their carbon support, they become inactive, leading to irreversible ECSA loss. In addition, a reversible loss of ECSA is often described in the AFC literature (some AFC data showing that reversible degradation can be recovered by voltage pulsing or KOH

replenishment[2,20]). In that case, comparing the polarization curve after stop/restart and the steady state performance of the AFC can provide information on the total recoverable voltage loss from multiple degradation factors: water management, carbonation, etc., including catalyst surface poisoning.[2] However, this understanding is only partial and ECSA losses are rarely connected to a possible decrease of HOR performance. To further capture the degradation mechanisms of monometallic carbon-supported PGM catalysts in alkaline environments, the first part of this paper will unveil the proportion of irreversible ECSA loss (e.g. by nanoparticles detachment, dissolution or Ostwald ripening) and reversible ECSA loss (e.g. by "CO like" poisoning) of such catalysts upon prolonged HOR operation in model conditions. This will mimic their fate at membraneless AFC anodes. To that goal, real CO-stripping and (pseudo) "CO-like" stripping experiments will be used to differentiate the poisoned portion of the surface during AST *versus* the non-poisoned portion, isolate the fraction of reversible and irreversible ECSA losses, and connect these to their ability to maintain (or not) their HOR performance, measured in rotating disk electrode configuration.

One can argue that membraneless AFC or AEMFC anode catalyst are often not monometallic PGM/C nanoparticles. Bimetallic (and often bifunctional) catalysts are indeed popular in the alkaline fuel cell community, because these can show better activity and/or durability. For example, the group of Zhuang[21] proposed to use PtRu/C anode catalysts, owing to the faster HOR at these alloyed nanoparticles *versus* Pt/C ones, at least at operating temperatures below 80°C. Dekel *et al.*[22] reported Pd-CeO_2/C HOR catalysts for the HOR in alkaline media, that reached 1.4 W cm^{-2} of power density in an anion exchange membrane fuel cell (AEMFC). Sankar and co-workers[23] used Pd-Ni alloy nanoparticles supported on two different carbons for the formate oxidation reaction in alkaline media: an enhanced mass activity of 4.5 A mg^{-1} compared to 1.5 A

mg^{-1} from Pd/C, was reported. Zhuang *et al*. found that Pd-$Ni(OH)_2$ composite electrocatalysts had a positive bifunctional effect on the alkaline HOR[24], the bifunctional effect scaling with the surface oxophilicities. Kiros and Schwartz observed the high durability of mixed of Pt + Pd catalysts (both supported on charcoal support, from Johnson Matthey Chemicals) when tested in a half-cell configurations, immersed in 6 M KOH and at 55°C.[25] This selected literature review shows the interest of bimetallic/bifunctional catalysts for alkaline oxidation reactions and in particular the HOR. However, besides the latter paper, little is known about the durability of such bimetallic surfaces in HOR operation, and even less about the possible existence of reversible/irreversible degradation pathways of such catalysts in alkaline HOR conditions. The literature does also not make clear whether their extent of ECSA loss in prolonged HOR operation and/or AST may affect (or not) their HOR activity. The second part of the paper will fill this gap; it evaluates two bimetallic catalysts from GenCell, Israel (these consist of Pd-Pt/C and Pd-Ni/C, using a proprietary carbon and small PGM content), and compares their HOR performance and durability to that of the commercial monometallic catalysts studied in the first part of the paper. Lastly, the GenCell bimetallic catalysts are also evaluate in real AFC stack operation.

2. Materials & Methods

Benchmark monometallic PGM/C catalyst were purchased at commercial providers: 20wt.%Pd/Vulcan XC72 from Premetek and 20wt.% Pt/Vulcan XC72 from E-TEK. GenCell provided bimetallic catalysts: Pd-Ni/C and Pd-Pt/C, the materials being proprietary, but containing low wt.% of each PGM (typically below 5 wt%) *vs* C and 17.5wt.% Ni *vs* C. Their synthesis is described in a recent patent[26].

For the rotating disk electrode (RDE) measurements, catalysts inks were prepared in the same way for all these catalysts, by mixing the required amount of the catalyst powder in 3000 µL of ultrapure water (18.2 MΩ cm, < 3 ppb Total Organic Carbon, TOC), 2000 µL of isopropyl alcohol (IPA), 20 µL of Nafion® solution (5wt.% in water-light alcohol mixture). This suspension was sonicated in an ultrasonic bath for 2 h until homogeneous and then deposited on the surface of a 5 mm-diameter glassy-carbon RDE to yield 10 µg total PGM cm^{-2}. The RDE was previously polished with diamond paste of 6, then 3 and 1 µm and rinsed thoroughly with IPA and ultrapure water.

The three-electrode cell experiment was carried out in 0.1 mol L^{-1} KOH aqueous solution (KOH Alfa Aesar) and was purged by Ar to remove all O_2 in the solution; the temperature was held at T = 25°C during the measurements. The counter electrode was a glassy carbon plate, the reference electrode was a reversible hydrogen electrode (RHE) in a PTFE tube (Hydroflex) and all this system was controlled by a numerical potentiostat (VSP®, Biologic) using the EC-Lab® software. The cell comprised a PTFE beaker to avoid direct contact of the corrosive alkali solution with Pyrex glass.

In the electrochemical measurements, three different drop-casts were tested for 3 series to yield an accurate calculation of ECSA before and after AST. The first set was used to study the PdO_x and/or PtO_x reduction peaks and/or Ni^{2+} to Ni^{3+} redox of the pristine catalysts, both can be observed by sweeping the potential to 1.5 V *vs* RHE (Figure SI 1 & 2). The second set was used to study the HOR performance and the third set was used to perform "CO-like" stripping experiments, before and after AST (Figure SI 3, 4 & 5 show the first 2 cycles of typical "CO-like" stripping experiments). All three drop-casts series were characterized as follows. 1) Stabilization cyclic voltammetry (CV) in Ar was performed at a sweep rate of 20 mV s^{-1} in the potential range from

0.05 to 1.05 V *vs* RHE (stability of the CV plot is usually reached within 20 cycles). 2) Three cycles of CVs were then recorded from 0.05 to 1.5 V *vs* RHE, at a sweep rate of 20 mV s^{-1}. This way, the different effects on the ECSA/properties of each catalyst can be observed from different testing procedures and gas environments. For the detailed testing steps of HOR-set and CO-set, the reader can refer to the supporting information, Table SI 1 & 2. In any case, Ohmic-drop was evaluated and corrected in a dynamic manner (at 85%) for all experiments. The ECSA calculated based on 1. CO stripping or "CO-like" stripping, 2. PdO_x and PtO_x reduction peaks and 3. Ni^{2+} to Ni^{3+} redox peaks were determined by calculating the area under the corresponding peaks. The charge-density in each case was considered to yield the area (in cm^2) of PGM. They are 1. 420 μC/cm^2, 2. 424 μC/cm^2 and 3. 514 μC/cm^2, respectively.

The hydrogen oxidation reaction (HOR) characterizations were carried out in hydrodynamic conditions in H_2-purged electrolyte (saturated by 30 min H_2 purge) using the rotation speed of 400, 900, 1600 and 2500 rpm; In each case, 2 CVs were plotted at 5 mV s^{-1} in the potential range 0 to 0.5 V *vs* RHE. Mass activity (MA) and Specific activity (SA) were derived from such measurements. The values were determined at 10 mV *vs*. RHE and corrected from mass-transport limitation using the Levich method.

AST experiments consisted of repeated CVs in the potential range from 0.1 to 1.23 V *vs* RHE, at a sweep rate 100 mV s^{-1} in Ar atmosphere. We particularly applied 150 cycles in these conditions, so to compare with earlier studies of the group. [16–18]

The "CO-like" stripping experiment was performed after the above-mentioned AST, and was designed to have 2 steps, to unveil the reversible and irreversible ECSA losses. In step 1, a blank (or fake, or pseudo) CO-stripping was measured, where Ar purge was applied for 45 min while the electrode potential was held at 0.1 V *vs* RHE, after which 3 cycles of CVs were plotted

in the potential range 0.05 to 1.05 V *vs* RHE. Step 2 consists of a real CO-stripping: while the potential was held at 0.1 V *vs* RHE, CO was purged for 6 min, and then Ar was purged for 39 min to remove any excess CO, after which 3 cycles of CVs were plotted in the potential range 0.05 to 1.05 V *vs* RHE.

The crystallite size was characterized by X-ray diffraction (XRD) for each catalyst powder. The XRD patterns were obtained using a PANalytical X'Pert PRO MDP apparatus with an λ = 0,15419 nm $K\alpha$Cu excitation beam. The scans were performed with a sweep rate of 0.1° min^{-1} in a range 2θ = 8-120°.

In order to evaluate the morphology of the catalysts, transmission electron microscopy (TEM) and identical location TEM (ILTEM) were carried out with the fresh ink of the catalysts (deposited on an Au-Lacey-carbon grid) and after the AST. The microscope used was a JEOL 2010, with a LaB6 filament operated at an acceleration voltage of 200 kV, leading to a point-to-point resolution of 0.19 nm.

As a final validation, durability test of a full cell module comprising 24 cells (see Figure SI-6), with a geometric area of 270 cm^2 for each electrode was conducted at GenCell. Each individual cell consists of anode and cathode chambers, where hydrogen and air are flowing, respectively. The cathode is fed in a constant air flow mode and the anode by repetitive pulses of hydrogen, supplied every few minutes. The catalysts are Pd-Ni/C or Pd-Pt/C for the anode and porphyrin-based for the cathode. They were employed in gas diffusion electrodes prepared according to GenCell patent[27]. The electrolyte is a 30% KOH aqueous solution at a temperature of 70°C; it is circulated in the opposite direction of the gases. The durability test lasted several 100 hours under load, during which the performance of the module was measured by a polarization

curve every 24 h. The power was extracted from such curve at a current of 100 A. It was plotted against the operation time, which is the net time of the module under load.

3. Results and discussions

3.1. Monometallic PGM/C catalysts

The degradation of monometallic carbon supported PGM nanoparticles in alkaline media has already been studied in a great extent, especially for Pt/Vulcan XC72 and Pd/Vulcan XC72. [16–18,28,29] These catalysts are often used at the anode of an AFC (HOR side); it is known that for practical AFCs, the anode can experience potential values as low as 0 V *vs* RHE (start – under H_2) and as high as 1 V (stop – under air), thereby resulting in frequent cycling between low and high potential values.[2] Since the degradation of the reactions kinetics is controlled by the operational temperature, applied potential and carbon support's properties (among others), the testing procedure for 20% Pt/Vulcan XC72 and 20% Pd/Vulcan XC72 was kept the same all throughout; hence, the chosen accelerated stress test protocol was set as 150 cycles of CVs between 0.1 and 1.23 V *vs* RHE in 0.1 mol L^{-1} KOH. For such conditions, Figure 1 A, B confirms that these catalysts greatly degrade in only 150 cycles of AST in 0.1 M KOH, with a clear suppression in all redox peaks; this agrees with previous studies of the group.[16–18,28] Lafforgue *et al.* and Zadick *et al.* also studied different loading of Pd on Vulcan XC72 or on graphene nanosheets[30] and concluded that Pd degrades less than Pt in alkaline media.[16] In detail, the CO-stripping experiment before and after AST in Figure 1 C, D confirms their result: 48 % loss of ECSA for Pd *vs* 52 % for Pt (Table 1). In these earlier studies, most of the ECSA loss was ascribed to the irreversible major detachment

and/or agglomeration of the PGM nanoparticles from their carbon support, and by minor Ostwald ripening and resulting particles growth (*i.e.* particle dissolution and redeposition).[31,32]

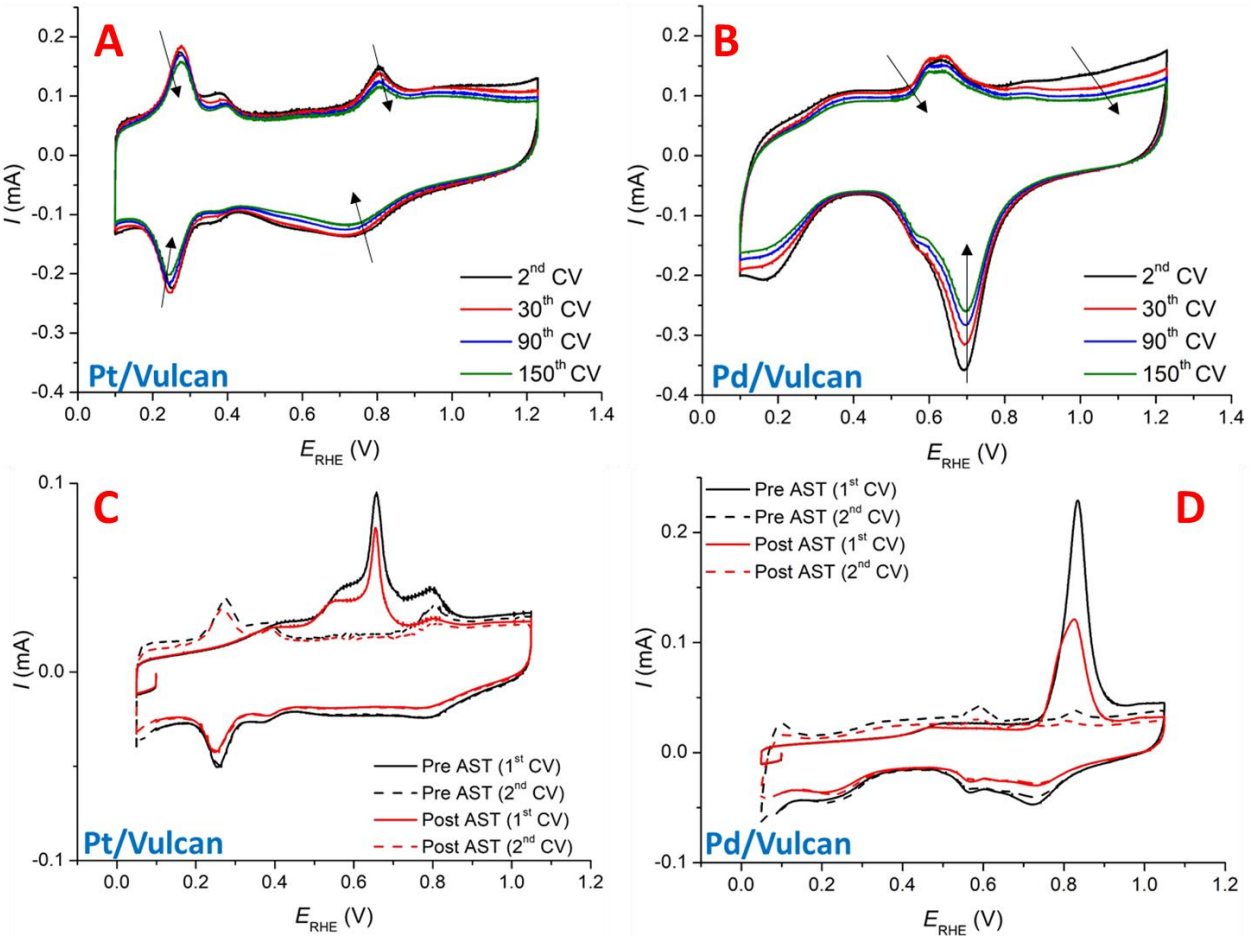

Figure 1: Accelerated Stress Test (AST) (A, B) and CO-stripping pre and post AST (C, D) for **20wt.% Pt/Vulcan XC72 and 20wt.% Pd/Vulcan XC72** . Condition: AST in 0.1 mol L^{-1} KOH, @25°C, Ar, [0.1 ,1.23] V *vs* RHE @ 100 mV s^{-1} , 150 cycles of CVs. CO stripping: hold at 0.1 V *vs* RHE for 6 min while purging CO, then switch to Ar for 39 min while still holding @ 0.1 V *vs* RHE . m_{PGM} = 10 µg cm^{-2}.

Because the detachment and/or agglomeration of the PGM nanoparticles is related to the propensity of the PGM nanoparticles to catalyze the oxidation of the carbon oxygenated surface groups[16], one may question whether some of the ECSA loss monitored after such AST could be due to the back-spillover of CO_x-like species formed on the carbon surface at potential above ca. 0.2 V *vs* RHE to the reduced platinum surface (Pt is reduced below ca. 0.6 V *vs* RHE). This process would poison/block the corresponding Pt surface for any reaction, and in particular regarding the hydrogen underpotential deposition, which is used in Figure 1 to probe the ECSA. Castanheira *et al*. indeed suggested this scenario, for experiments performed in acidic environments (0.1 mol L^{-1} H_2SO_4) [31,32], but it has never been demonstrated for tests performed in alkaline conditions. For acidic conditions, Castanheira *et al*. explained that, for potential below 0.8 V *vs* RHE (in acidic environment), CO-containing moieties (CO_x-groups) from surface groups of carbon (hereafter denoted as "CO-like" species) back-spill over from the carbon support to the Pt surface and block some portion of the active area. To test whether some catalyst surface poisoning happens also in alkaline environment and whether it is a reversible process, pseudo "CO-like" stripping (or blank CO-stripping) experiment have been attempted after the above-mentioned AST procedure.

During a blank CO stripping, only Ar is purged for 45 min while the potential is maintained at 0.1 V *vs* RHE, before the potential is scanned from 0.05 to 1.05 V *vs* RHE for 3 cycles. Figure 2 A, B presents the comparison of such a blank CO-stripping (without CO) and the real CO-stripping (with CO) of the 20% Pt/Vulcan XC72, measured before and after AST. As shown in Figure 2 A, the 1st cycle of the CO-stripping experiment (red plot) for the pristine Pt surface (before AST) has a typical response; it corresponds to the initial ECSA of the catalyst (active area from CO-stripping: $S_{Pt\text{-}CO/CO\text{-}preAST}$ = 0.50 cm^2) and none of the Pt surface was detected in the H-UPD region at that stage ($S_{Pt\text{-}H/CO\text{-}preAST}$ = 0 cm^2); similarly, the 1st cycle of the blank CO-stripping corresponds to a clean surface (free from CO: $S_{Pt\text{-}CO/BlankCO\text{-}preAST}$ = 0 cm^2): the whole usual features of Pt are visible

(hydrogen UPD and Pt oxide regions), and the active area from H-UPD is $S_{Pt\text{-}H/BlankCO\text{-}preAST}$ = 0.50 cm^2 (equal to $S_{Pt\text{-}CO/CO\text{-}preAST}$). After AST, the blank CO-stripping experiment of Figure 2 B shows that the Pt surface is divided in 2 contributions; some of the surface was still available in the H-UPD region and therefore not poisoned (ECSA 1: $S_{Pt\text{-}H/BlankCO\text{-}postAST}$ = 0.12 cm^2), while another portion of the Pt surface was covered by "CO-like" species and is freed at higher potential in a CO-like-stripping peak (ECSA 2: $S_{Pt\text{-}CO/BlankCO\text{-}postAST}$ = 0.12 cm^2). Thus, the total ECSA of the Pt/Vulcan post AST is the sum of the free surface (ECSA 1) and of the poisoned surface (ECSA 2): $S_{Pt\text{-}total/BlankCO\text{-}postAST}$ = 0.12 + 0.12 = 0.24 cm^2. This is the exact value of ECSA 3 (Table 1), measured by real CO-stripping after the AST: $S_{Pt\text{-}CO/CO\text{-}postAST}$ = $S_{Pt\text{-}total/CO\text{-}postAST}$ = 0.24 cm^2 (because $S_{Pt\text{-}H/CO\text{-}postAST}$ = 0 cm^2). Of course, once the CO-like groups that were present before the blank CO-stripping have been stripped in the 1st cycle, the Pt surface becomes fully available for the H-UPD process in the 2nd cycle (Figure 2 C): the value of H_{upd} from the second cycle of the blank CO-stripping is the same as ECSA 3 (= ECSA 1+ ECSA 2). The fact that post-AST, the Pt surface is partially covered by CO-like species (ECSA 2) is a direct evidence that indeed, Pt is capable to adsorb the CO_x-groups of the carbon substrate, and that these CO-like species can be stripped at higher potential value in the well-known Langmuir-Hinshelwood mechanism. This further confirms that Pt catalyzes the Carbon Oxidation Reaction (COR), even in alkaline environments. It is worth to add that this poisoning is reversible, provided the electrode is scanned to high-enough potential to strip the CO-like species. Under the described condition, Pt can be poisoned up to 50% by the "CO-like" group.

In short, this experiment not only provides a quantitative evidence for the recoverable catalysts surface poisoning, which is often witnessed in running AFCs[2,20], but also confirm the short-coming of the carbon-supported monometallic Pt catalyst, which suffers the highest amount

of irreversible loss among the four catalysts in this study (ca. 52%, assuming the aged catalyst ECSA: $S_{Pt\text{-}CO/CO\text{-}postAST}$ = 0.24 cm^2 *vs* the initial one: $S_{Pt\text{-}CO/CO\text{-}preAST}$ = 0.50 cm^2).

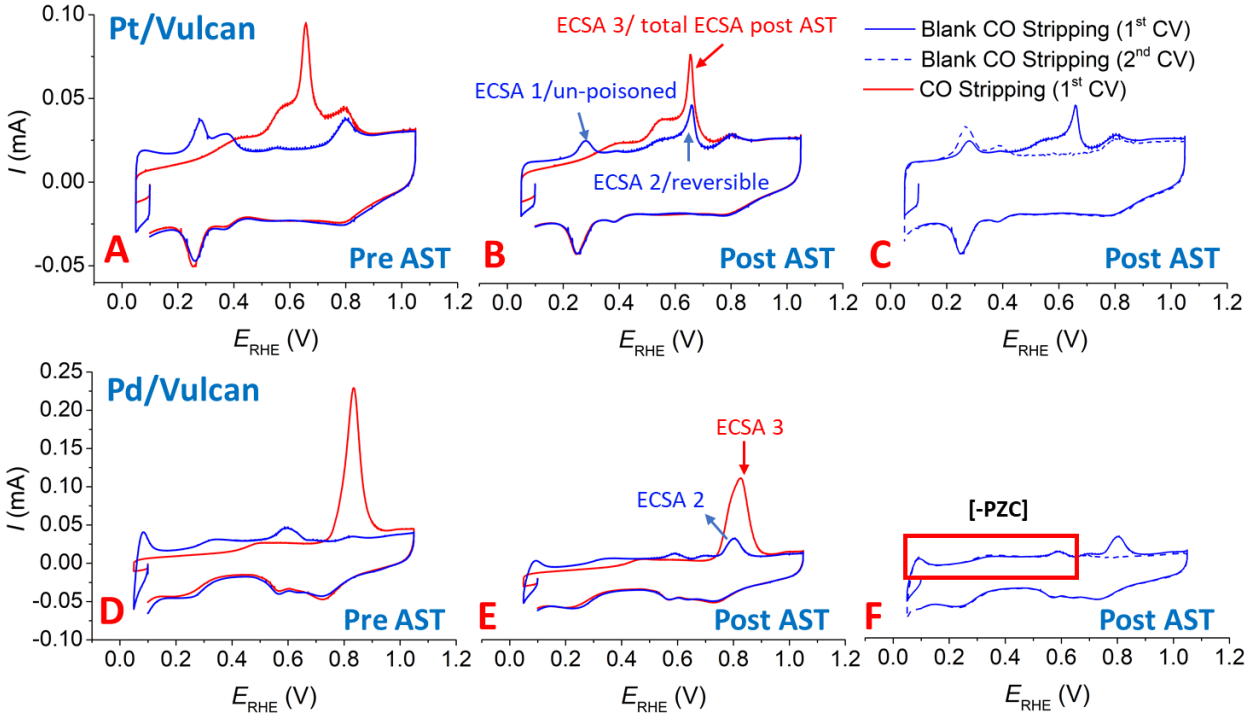

Figure 2: "CO like" stripping of **Pt/Vulcan (A-C) and Pd/Vulcan (D-F)**; comparison of the 1st cycle of a blank CO-stripping (without CO – blue plot) and the real CO-stripping (with CO – red plot) measured (A,D) before and (B,E) after the AST; (C,F) comparison of the 1st (solid line) and 2nd (dashed line) cycle of the blank CO-stripping performed after the AST.

Similar to Pt/Vulcan, Pd/Vulcan also had the same and usual response from the first cycle of its CO-stripping experiment (red plot, Figure 2 D). The ECSA of the pristine Pd was $S_{Pd\text{-}CO/CO\text{-}preAST}$ = 1.57 cm^2 and the region negative to the potential of zero-charge ([-PZC]) showed suppressed feature of H-UPD and Pd-hydride (Pd-H$_x$)[33]. Because of this combined features, the literature states that calculating the ECSA of Pd using CO-stripping and PdO$_x$ reduction can be

more accurate than using [-PZC] region. [34,35] This uniqueness of the Pd's [-PZC] region leads to an unclear calculation of the reversible surface area loss, as well as different features in the blank CO-stripping experiment, unlike for Pt. In details, although the first cycle of the blank CO-stripping pre AST (Figure 2 D) is still the clean surface (free from CO: $S_{\text{Pd-CO/Blank CO-preAST}} = 0$ cm^2), as the usual features of Pd are visible in the [-PZC] region, the first cycle of the blank CO-stripping post AST (Figure 2 E) has two contributions, just like for Pt. The two contribution are ECSA 1 = $S_{\text{Pd-[-PZC]/Blank CO-post AST}}$ and ECSA 2 = $S_{\text{Pt-CO/BlankCO-postAST}}$. The total ECSA remaining post AST is not simply equal to ECSA 1 (area of [-PZC] region) + ECSA 2, due to the unknown contribution of palladium hydride (Pd-H_x) in the [-PZC] region, so ECSA 1 could be a sum of ECSA 1' and ECSA 1'', where ECSA 1'= $S_{\text{Pd-H/Blank CO-post AST}}$ and ECSA 1''= $S_{\text{Pd-Hx/Blank CO-post AST}}$. As the result, Figure 2 F shows no clear poisoned portion of the Pd surface from the first cycle (solid line) and almost no regaining in the [-PZC] in the second cycle (dashed line). Based on the value of ECSA 2 = $S_{\text{Pt-CO/BlankCO-postAST}} = 0.154$ cm^2, which is only ca. 19% *vs*. the total remaining ECSA 3 = $S_{\text{Pd-CO/CO-postAST}} = 0.82$ cm^2, it could be concluded that the $S_{\text{Pd-H/Blank CO-post AST}}$ is about 81% *vs*. ECSA 3 (ECSA 3 = ECSA 1' + ECSA 2 and so ECSA 1' = ECSA 3 - ECSA 2). Assuming the much lower amount of "CO_x-like" species produced under the same condition in the case of Pd than Pt, plus the lower total irreversible loss for Pd ($S_{\text{Pd-CO/CO-preAST}} = 1.57$ cm^2 *vs.* $S_{\text{Pd-CO/CO-postAST}} = 0.82$ cm^2), one can clearly conclude that Pd catalyzes the COR with significantly slower rate than Pt does. This result was not a surprise, since it confirms similar finding from the previous studies on Pt *vs*. Pd.[16,28,36]

The loss of ECSA of the two catalysts is a good marker of their degradation upon an AST. Their activity for the HOR is no less important to quantify. Figure 3 A shows a big drop in HOR

performance of Pt post AST (here, it must be stated that the catalysts were not pre-activated prior measuring their HOR activities at any stage, *i.e.* not pre-reduced, as often performed in the literature). This large loss aligns with the conjunction of the large reversible and irreversible ECSA loss of 52%. In addition, it is worth adding that the HOR kinetics also degrades within 2 successive cycles of CV conducted between 0 and 0.5 V *vs* RHE from 400 rpm to 900 rpm to 1600 rpm to 2500 rpm (in this chronological order), even at the initial state (*i.e.* before the 150 cycles of AST); this loss of activity is too fast to be due to major irreversible degradations and points towards gradual poisoning of the Pt surface when it is maintained in the "low potential" range (typically between 0 and 0.5 V *vs* RHE, *i.e*. potential values where CO_x-species can form on carbon and spill-over to the reduced Pt surface to poison it). This means that Pt is very active to promote the oxidation of its neighboring carbon support. Of course, the loss of the HOR performance is more severe after the AST, as shown in the low overpotential window [0 to 0.05 V *vs* RHE], where the current of 2500 rpm nearly overlaps with that at 1600 rpm. Figure 3 B shows the same trend for Pd but at a much faster rate, even though it has less percentage ECSA loss. In addition, Figure 4 A, B shows that the kinetic current of Pd pre-AST stage, based on its PGM mass or initial ECSA, is much lower than for Pt: the percentage HOR current loss post AST of Pd (78%) is greater than for Pt (61%). When analyzing the specific activity (SA) of HOR pre and post AST according to their ECSA measured pre and post AST (Figure 4 C), the same trend is witnessed: 58% loss for Pd and 19% for Pt.

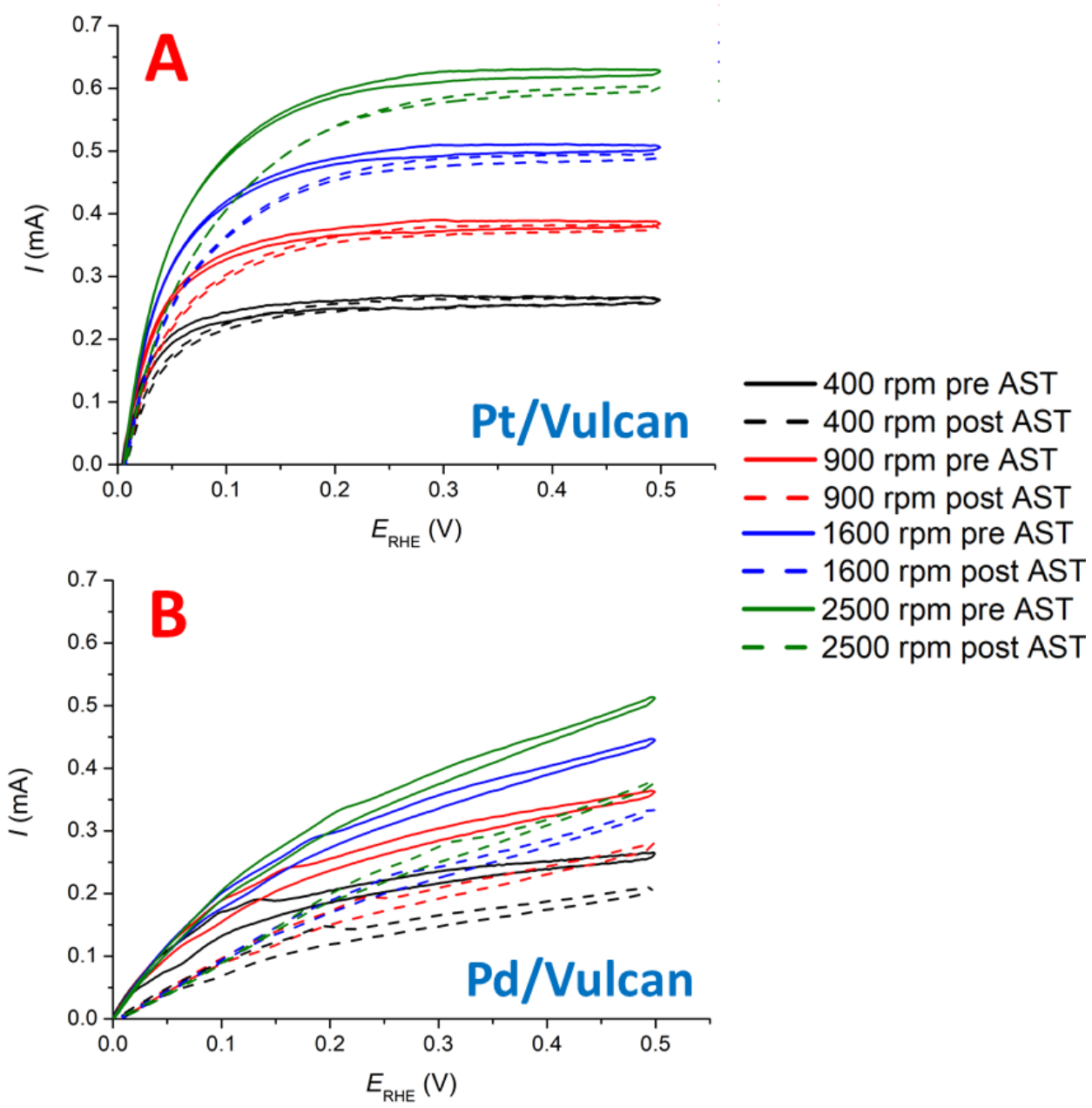

Figure 3: HOR performance of **Pt/Vulcan (A) and Pd/Vulcan (B).** 5 mV s^{-1} , 2 cycles of CV are performed at each rotation speed.

Table 1: ECSA measured from CO-stripping CVs

Material	ECSA Pre AST-1 (cm^2)	ECSA Post AST-1 (cm^2)	% PGM ECSA loss (irreversible loss)
Pt	0.50	0.24	52
Pd	1.57	0.82	48
Pd-Pt	1.61	0.94	42
Pd-Ni	**0.90**	**0.77**	**14**

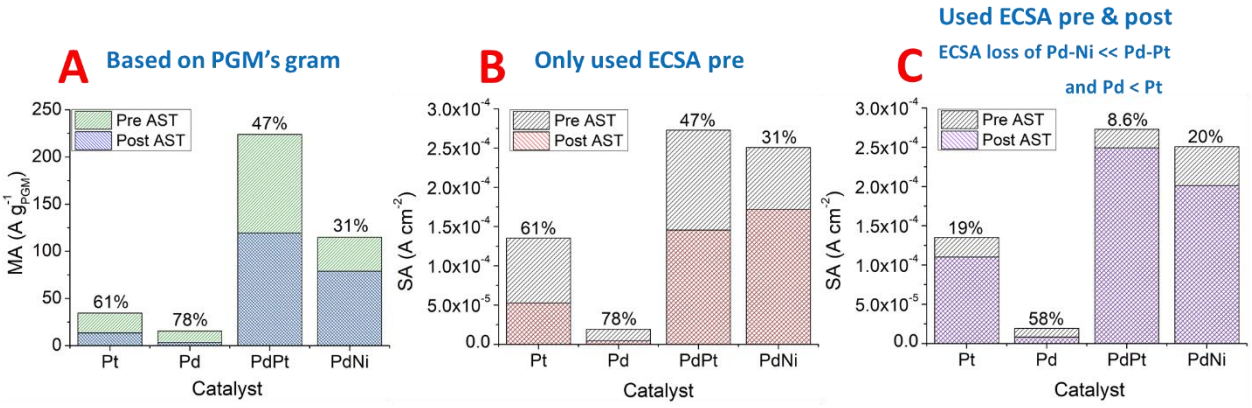

Figure 4: Mass activity (MA) and and specific activity (SA) analysis of **Monometallic *vs.* Bimetallic** catalysts. The percentage values over each bar-graph indicate the losses of activity upon the AST for the individual catalysts. In each case, the SA and MA values were determined at 10 mV *vs*. RHE and corrected from Ohmic drop and mass-transport limitation.

3.2. Bimetallic PGM/C catalysts

From the XRD patterns of Pd-Pt/C and Pd-Ni/C (Figure SI 7), it is not possible to state if the Pd-Pt is constituted of alloyed or composite nanoparticles, due to the low PGM loading (hereafter, noted LD) on carbon and low crystallinity, small size and very similar expected patterns for Pt and Pd. XPS data, not shown, did not enable more conclusive results. For Pd-Ni, clear

patterns for Pd, PdNi, Ni and $Ni(OH)_2$ are observed, showing that the nanoparticles cannot be considered as perfectly alloyed, even at initial state. Both catalysts contain silicate impurities in a small amount, which is coming from the carbon support (C). These features are confirmed by TEM (Figure 6) for the initial samples, overall.

The AST results of the bimetallic PGM/C catalysts in Figure 5 clearly evidence their slow degradation compared to the monometallic PGM/C catalysts. Since Pd-Pt/C and Pd-Ni/C both have a big double layer feature, coming from their high C and/or Ni contents, the actual degree of suppression in all redox peaks might not be the best way to compare them with the monometallic catalysts. Fortunately, the percentage of ECSA loss can still be accurately calculated using the CO-stripping technique (Figure 5 C, D and Table 1). Although the AST-CV of Pd-Pt/C led to minor changes compared to the monometallic catalysts (Figure 1 A, B), its percentage of ECSA loss is quite high: 42% and is only 10 points% less than Pt/C and 6 point% less than Pd/C values post AST (Table 1). The IL-TEM of Pd-Pt/C (Figure 6 A) also suggests that this catalyst did neither suffer high degree of agglomeration nor nanoparticles detachment: the percentage of nanoparticles loss is only 27%, counted for ca. 200 nanoparticles on 200K-magnified micrographs. As mentioned above, Kiros and Schwartz showed that the Pt + Pd mix had higher survival rate in 6 mol L^{-1} KOH and at 55°C than equivalent monometallic catalysts, but they did not have an explanation for why. The present results show that combining Pd-Pt (1-1) leads to slower degradation rate compared to Pt alone, and this is due to the presence of Pd, which was proven to be degraded slower than Pt[16]. However, the reason why Pd-Pt degrades less than Pd is unclear, so far, even though one could point that the presence of more oxophilic Pd in the vicinity of Pt atoms/particles could make the Pd-Pt material less prone to be fully reduced at low potential. Hence this bimetallic catalyst is less susceptible to accept CO_x groups from carbon (which need reduced metal/alloy surface to adsorb

on the particles), thereby lowering its catalytic effect on carbon corrosion during the AST. Better understanding of the degradation mechanism of such catalyst *vs*. monometallic ones would require that future experimentalists spend more time on this issue, e.g. by fixing the metals loading *vs*. carbon for monometallic and bimetallic or fixing the carbon support, which is not the primary outcome of the present paper.

To enable easy comparison of the performance of Pd-Pt/C and Pd-Ni/C, the PGM loading *vs*. C support was fixed between them. Clearly, both catalysts work much better than the standard commercial monometallic catalysts, and Pd-Ni/C is the least affected during AST with only 14% percentage of ECSA loss (Table 1).

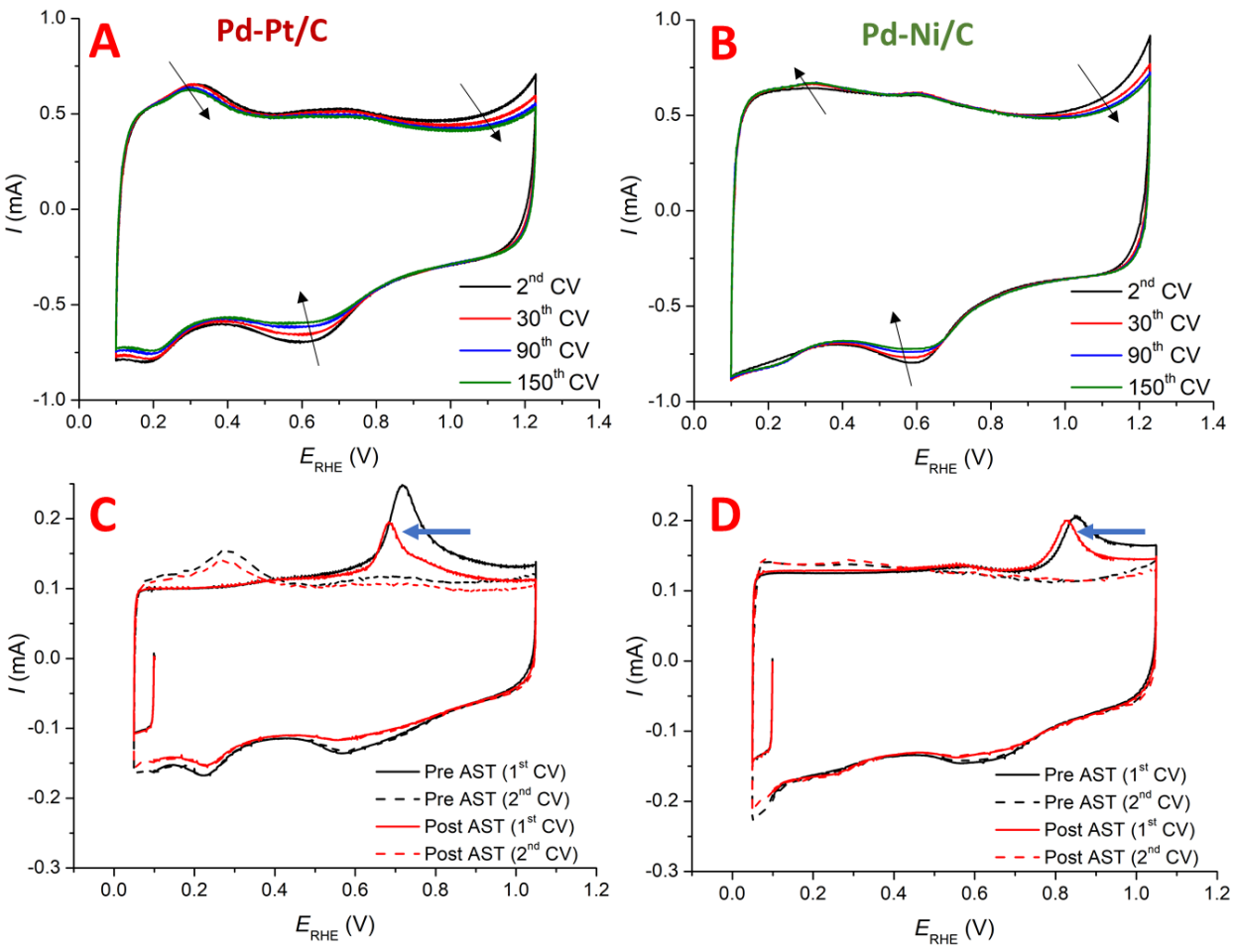

Figure 5: Accelerated Stress Test (AST) (A,B) and CO stripping pre and post AST (C,D) for **Pd-Pt/C and Pd-Ni/C** accordingly. Conditions are identical to Figure 1.

The IL-TEM of Pd-Ni/C (Figure 6 B) provides a big picture of how this type of catalyst behaves upon AST (same for Pd-Pt/C). Unlike Pd-Pt/C, Pd nanoparticles in this case were not as affected post AST (neither irreversible detachment nor dissolution has been detected). One of the obvious reasons is that there are fewer nanoparticles on the carbon support (they are bigger) compared to Pd-Pt/C (regardless that the PGM loading was kept the same for each drop-cast). Figure 5 B, D also confirm the "mostly pristine stage" of Pd in Pd-Ni/C post AST, based on the minimal changes in the AST-CV pattern or the size/shape of CO stripping peak. The CO-stripping peak in the case of Pd-Pt/C-post AST (Figure 5 C) shifted more to the left compared to Pd-Ni/C-post AST (Figure 5 D). Larger negative shift could indicate that the PGM was more oxidized in Pd-Pt/C, and that greater extent of agglomeration or larger particle size growth occurred upon the AST [37,38]. Similar conclusion can be drawn when examining the area of the PGM-O_x reduction peak pre and post AST (Figure SI 1 A, B). The negative shift of this peak in the case of Pd-Pt/C was also larger than for Pd-Ni/C, because the Pd-Pt nanoparticles were more oxidized during AST and need larger cathodic overpotential to be reduced. Table SI 3 presents the percentage ECSA loss of this reduction peak and once again confirms that Pd-Ni/C has the least amount of PGM loss (only 9.05%). In addition, by going up to 1.5 V *vs* RHE, both ECSA of the PGM-O_x reduction peak and NiO_x reduction peak can be calculated. The IL-TEM images from Figure 6 B (red box) and Figure SI 1 C suggests that the $Ni(OH)_2$ needles grow double in size post AST and the value of NiO_x reduction peak from Table SI 4 confirms the overall value in a single drop-cast. It can be concluded that the presence of Ni enables to somewhat stabilize Pd, because it is more oxophilic

compared to Pd, as also pointed out by Zhuang *et al.*[24]. Ni therefore plays the role of "sacrificial anode" and protects Pd: upon oxidation, Ni forms stable oxides and self-protects from alkaline corrosion/dissolution and so overall, Pd-Ni is the most stable combination in this study.

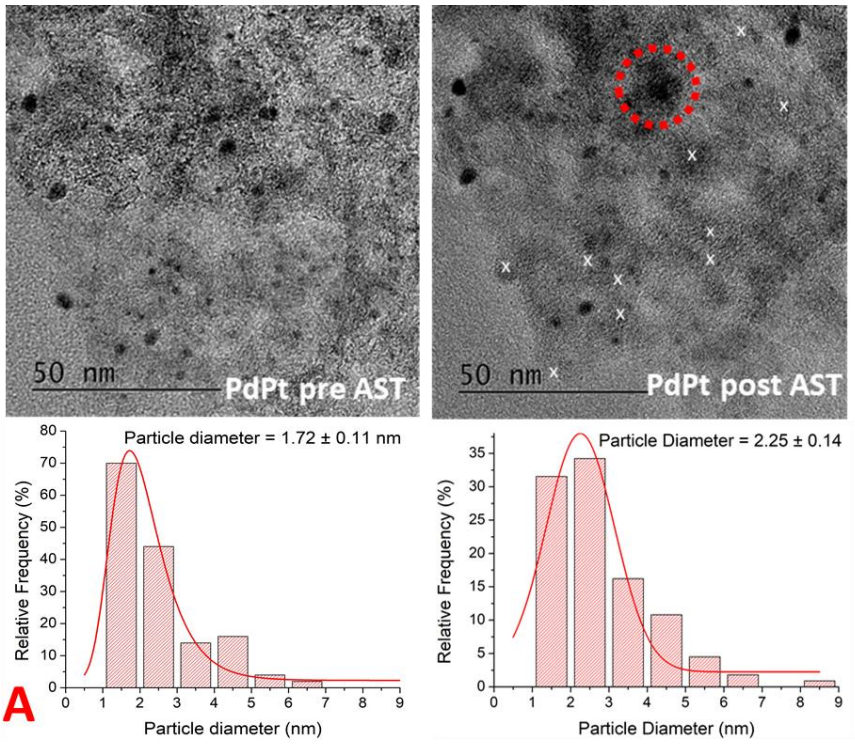

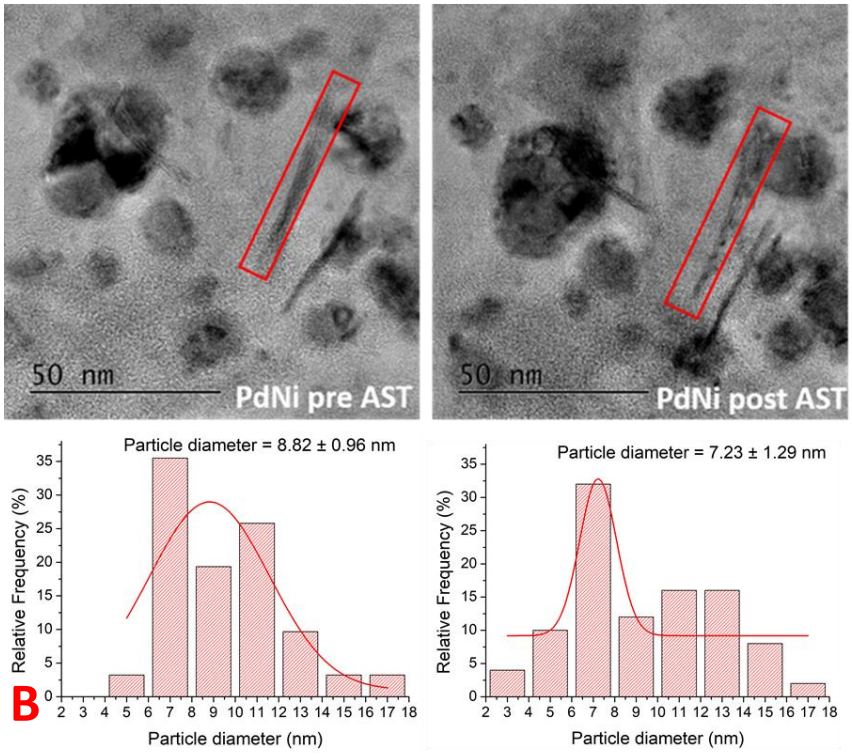

Figure 6: IL-TEM and particle distribution of **A. Pd-Pt/C and B. Pd-Ni/C**. The dashed red circle in (A) indicates particles growth, whereas the red rectangles in (B) show that the $Ni(OH)_2$ needles grow and crystallize after AST. In any case, the white crosses highlight some particles detachment/dissolution (the markers not being comprehensive).

Not only the bimetallic catalysts have lower ECSA loss, but Figure 7 A, B also shows their higher HOR activity survial rate -post AST- compared to the monometallic ones. Again, this can be explained by the "CO like" stripping experiment, presented in Figure SI 5. In contrast with the monometallic catalysts, the bimetallic ones showed minimum or no "CO-like" species stripping peak in these pseudo CO-stripping experiment. Since they do not lead to real COR promotion, they are not subjected to consequent reversible loss of ECSA, so $S_{\text{Pd-Ni-CO/BlankCO-preAST}} \approx S_{\text{Pd-Ni-CO/BlankCO-preAST}} \approx S_{\text{Pd-Pt-CO/BlankCO-preAST}} \approx S_{\text{Pd-Pt-CO/BlankCO-preAST}} = 0$. In consequence, their irreversible losses

would just be the differences between ECSA pre and post AST (values from Table 1) and the irreversible percentage losses are 42% for Pd-Pt/C and 14% for Pd-Ni/C, the latter having the lowest irreversible ECSA loss among the four tested materials.

The outstanding stability of HOR performance of Pd-Ni/C matched its maintained ECSA post AST, whatever the technique of its determination (the degradation and the percentage of ECSA loss is low from all methods: CO-stripping or PGM-O_x reduction peak coulometry). From Figure 7 A, B, one could argue that the better survival HOR current for Pd-Ni/C than for Pd-Pt/C could originate from bias in its determination, owing to the large double layer current measured for these materials. To rule out this uncertainty, Figure 4 shows the comparison of HOR mass activity and specific activity for all four catalysts, measured at 10 mV *vs* RHE, where the double layer contribution does not significantly interfere with the evaluation of the intrinsic activity. The clear trend of % losses of MA & SA-based on ECSA pre-AST (Table 1) is Pd > Pt > Pd-Pt > Pd-Ni (31% loss). When comparing the SA of the four catalysts using the matching ECSA pre & post AST, two important observations can be made: 1) The SA of Pt and Pd are smaller among the four catalysts, since their HOR activities are dictated by the amount of ECSA (direct proportional relationship). 2) The SA of Pd-Ni is higher than the SA of Pt and Pd-Pt, because its ECSA was not as affected in the AST (20% loss). The MA values also point towards the benefit of the bimetallic strategy, with particular emphasis for the Pd-Ni catalyst. In conclusion, Pd-Ni/C is the best compromise between the materials' cost and the retention of ECSA and HOR activity in long-term operation; it is therefore the most-suitable material for use in AFC anodes. The recent literature confirms this finding, as whether used for methanol electrooxidation, ORR or HOR, both Pd and Ni component present excellent activity in high pH solution[22,24,39–41]. Hence, combining them is

surely beneficial for AFC reactions, not speaking from the lower cost of these materials versus purely PGM-based ones.

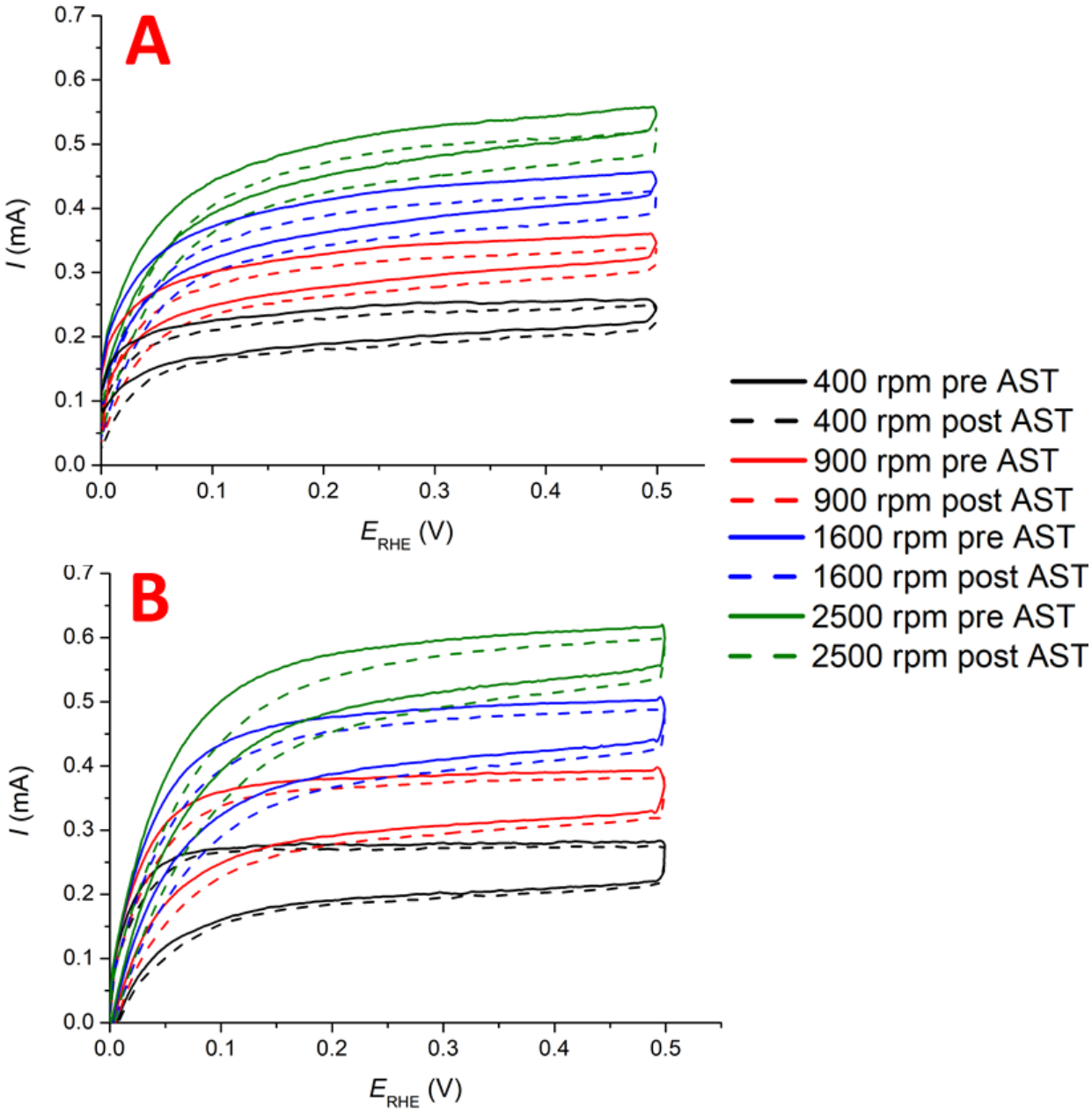

Figure 7: HOR performance of **Pd-Pt/C (A) and Pd-Ni/C (B).** 5 mV s^{-1}, 2 cycle of CVs are monitored at each rotation speed.

As a final validation of the bimetallic catalysts, Figure 8 shows the durability test of a full cell module comprising 24 cells, with a geometric area of 270 cm^2 for each electrode (see Figure SI 6 for the schematic of this module). The catalysts are either Pd-Pt/C or Pd-Ni/C for the anode and a carbon-supported porphyrin-based material for the cathode. Generally, for a commercial system, 16 modules are combined, that yield about 5 kW. The plot of Figure 8 shows the power of the module (sampled every 24 h at a current of 100 A) *versus* the operation time (the net time of the module under load). The data is from a current operating module started in early 2021. The cutoff value is 375 W in order to compare one experiment to another, but it can continue further if needed. As shown on Figure 8, the power of the module has a decay rate of 11%, from 1 h to 1053 h, in the case of Pd-Ni/C anode, which is slower than Pd-Pt/C anode (20%). Yet, such complicated full cell system is difficult to compare side by side between catalysts. It should be taken into consideration that the cell data is influenced by several factors, such as the cathode materials degradation, individual failing of each cell, flooding, etc.; thus, a meaningful statistic is pivotal to compare each anode catalyst. This being said, one nevertheless notes that both catalysts present high operational performance and durability for the HOR (even though their PGM content is small); Pd-Ni/C is a better choice in term of economic/performance compromise. It further demonstrates that the membraneless AFC technology from GenCell using Pt-free catalysts, *i.e.*, Pd-Ni/C, is a promising and advanced system for stationary power applications.

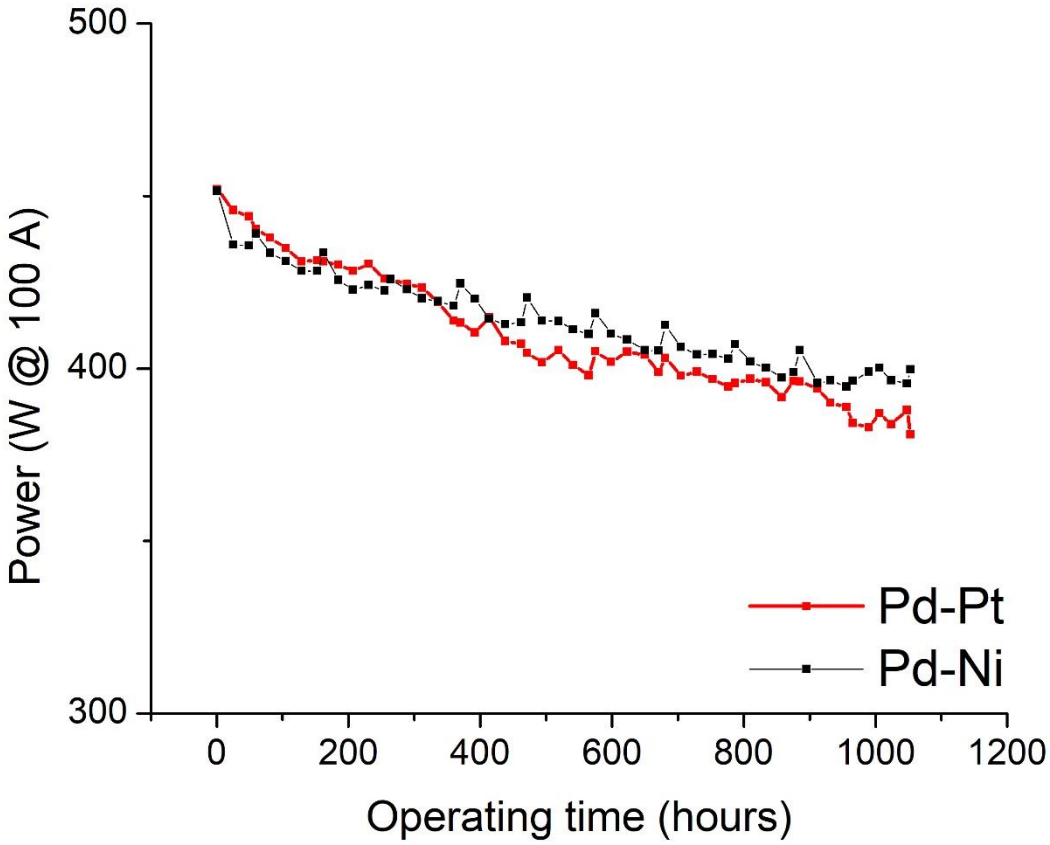

Figure 8: Durability test of a full AFC module, presented in terms of module Power at 100 A *vs.* Operating time. Anode catalyst: Pd-Pt/C vs. Pd-Ni/C and cathode catalyst: porphyrin-based. The electrolyte is a 30% KOH aqueous solution maintained at a temperature of 70°C, circulated in the opposite direction of the gases. All other parameters of the AFC module are similar for the 2 tests.

Conclusion

This work presents the very practical performance of Pd-Pt and Pd-Ni bimetallic HOR catalysts in high pH electrolyte. It particularly evaluates how these materials retain their ECSA upon an AST, using a combination of IL-TEM imaging and CO-stripping techniques to track their

reversible and irreversible degradations. The analyses include different ECSA calculation techniques (to calculate CO-stripping peaks, PGM-O_x reduction peaks and NiO_x reduction peak). The values from the "CO like" stripping methods and their confrontation to HOR kinetics measurements provide a clear explanation to why there are recoverable and unrecoverable voltage losses during AFC operation when using monometallic PGM materials. As the result, about 50% of Pt/C catalyst can be poisoned by the "CO_x-like" species that are produced during 150 cycles of AST, and only 19% for Pd/C. This was expected based on the larger propensity of Pt to assist carbon corrosion. Since the "CO_x-like" species can be removed by going to higher voltage (or voltage-pulsing in AFC set up), the ECSA loss caused by them is reversible (but leads to irreversible carbon corrosion, which on the long-term could have adverse consequences, like nanoparticles detachment or modification of the porous texture of the active layers. In the case of Pd-Pt/C and Pd-Ni/C, the reversible poisoning was not found major, sign of lesser extent of carbon corrosion. Hence, it is no surprise that both catalysts also have less particle detachment, less degraded ECSA and finally less affected HOR performance post AST. There is no doubt that Pd-Ni/C has the highest survival rate, with only 14% irreversible ECSA loss and 31% SA loss (based on ECSA pre AST); this bimetallic Pt-free catalyst therefore exhibits excellent durability and well-sustained HOR activity in alkaline environment, as practically demonstrated in a full cell AFC stack operated for *ca.* 1000 h with acceptable performance loss.

Acknowledgements

GenCell funded this research, and some of this work has been performed within the framework of the Centre of Excellence of Multifunctional Architectured Materials "CEMAM" n° ANR-10-LABX-44-01.

Authors' contributions

MC conceived the experiments, which were done by TM and HD and analyzed by HD, TM and MC. HD and TM wrote the first draft of the MS, which was reviewed and approved by all authors. MC finalized the contribution.

References

(1) Simon, C.; Hanzlik, M.; Gasteiger, H. A.; Schuler, T.; Durst, J.; Siebel, A.; Hasche, F.; Herranz, J.; Rheinlander, P. J. Hydrogen Oxidation and Evolution Reaction (HOR/HER) on Pt Electrodes in Acid vs. Alkaline Electrolytes: Mechanism, Activity and Particle Size Effects. *ECS Trans.* **2014**, *64* (3), 1069–1080.

(2) Mustain, W. E.; Chatenet, M.; Page, M.; Kim, Y. S. Durability Challenges of Anion Exchange Membrane Fuel Cells. *Energy Environ. Sci.* **2020**, *13* (9), 2805–2838.

(3) Dekel, D. R. Review of Cell Performance in Anion Exchange Membrane Fuel Cells. *J. Power Sources* **2018**, *375*, 158–169.

(4) Gülzow, E. Alkaline Fuel Cells. *Fuel Cells* **2004**, *4* (4), 251–255.

(5) Gouérec, P.; Poletto, L.; Denizot, J.; Sanchez-Cortezon, E.; Miners, J. H. The Evolution of the Performance of Alkaline Fuel Cells with Circulating Electrolyte. *J. Power Sources* **2004**, *129* (2), 193–204.

(6) Kordesch, K.; Gsellmann, J.; Cifrain, M.; Voss, S.; Hacker, V.; Aronson, R. R.; Fabjan, C.; Hejze, T.; Daniel-Ivad, J. Intermittent Use of a Low-Cost Alkaline Fuel Cell-Hybrid System for Electric Vehicles. *J. Power Sources* **1999**, *80* (1), 190–197.

(7) Peng, X.; Omasta, T. J.; Magliocca, E.; Wang, L.; Varcoe, J. R.; Mustain, W. E. Nitrogen-Doped Carbon–CoO x Nanohybrids: A Precious Metal Free Cathode That Exceeds 1.0 W Cm −2 Peak Power and 100 h Life in Anion-Exchange Membrane Fuel Cells. *Angew. Chemie - Int. Ed.* **2019**, *58* (4), 1046–1051.

(8) Wang, J.; Zhao, Y.; Setzler, B. P.; Rojas-Carbonell, S.; Ben Yehuda, C.; Amel, A.; Page, M.; Wang, L.; Hu, K.; Shi, L.; Gottesfeld, S.; Xu, B.; Yan, Y. Poly(Aryl Piperidinium) Membranes and Ionomers for Hydroxide Exchange Membrane Fuel Cells. *Nat. Energy* **2019**, *4* (5), 392–398.

(9) Sheng, W.; Gasteiger, H. A.; Shao-Horn, Y. Hydrogen Oxidation and Evolution Reaction Kinetics on Platinum: Acid vs Alkaline Electrolytes. *J. Electrochem. Soc.* **2010**, *157* (11), B1529.

(10) Durst, J.; Simon, C.; Hasche, F.; Gasteiger, H. A. Hydrogen Oxidation and Evolution Reaction Kinetics on Carbon Supported Pt, Ir, Rh, and Pd Electrocatalysts in Acidic Media. *J. Electrochem. Soc.* **2014**, *162* (1), F190–F203.

(11) Pourbaix, M. *Atlas of Electrochemical Equilibria in Aqueous Solutions. Houston:NACE International*, [1st Engli.; Pergamon Press: Oxford ;New York, 1974.

(12) Staud, N.; Ross, P. N. The Corrosion of Carbon Black Anodes in Alkaline Electrolyte: II . Acetylene Black and the Effect of Oxygen Evolution Catalysts on Corrosion. *J. Electrochem. Soc.* **1986**, *133* (6), 1079–1084.

(13) Ross, P. N.; Sokol, H. Corrosion of Carbon Black Anodes in Alkaline Electrolyte: I. Acetylene Black and the Effect of Cobalt Catalyzation. *Proc. - Electrochem. Soc.* **1984**, *84–5*, 313–343.

(14) Staud, N.; Ross, P. N. Corrosion of Carbon Black Anodes in Alkaline Electrolyte: Ii. Acetylene Black and the Effect of Metal Oxide Catalysts. *Electrochem. Soc. Ext. Abstr.* **1985**, *85–2*, 3–4.

(15) Staud, N.; Sokol, H.; Ross, P. N. The Corrosion of Carbon Black Anodes in Alkaline Electrolyte: IV . Current Efficiencies for Oxygen Evolution from Metal Oxide-Impregnated Graphitized Furnace Blacks. *J. Electrochem. Soc.* **1989**, *136* (12), 3570–3576.

(16) Lafforgue, C.; Zadick, A.; Dubau, L.; Maillard, F.; Chatenet, M. Selected Review of the Degradation of Pt and Pd-Based Carbon-Supported Electrocatalysts for Alkaline Fuel Cells: Towards Mechanisms of Degradation. *Fuel Cells* **2018**, No. 0, 1–10.

(17) Zadick, A.; Dubau, L.; Demirci, U. B.; Chatenet, M. Effects of Pd Nanoparticle Size and Solution Reducer Strength on Pd/C Electrocatalyst Stability in Alkaline Electrolyte. *J. Electrochem. Soc.* **2016**.

(18) Zadick, A.; Dubau, L.; Sergent, N.; Berthomé, G.; Chatenet, M. Huge Instability of Pt/C Catalysts in Alkaline Medium. *ACS Catal.* **2015**.

(19) Olu, P. Y.; Deschamps, F.; Caldarella, G.; Chatenet, M.; Job, N. Investigation of Platinum and Palladium as Potential Anodic Catalysts for Direct Borohydride and Ammonia Borane Fuel Cells. *J. Power Sources* **2015**, *297*, 492–503.

(20) Tomantschger, K.; Findlay, R.; Hanson, M.; Kordesch, K.; Srinivasan, S. Degradation Modes of Alkaline Fuel Cells and Their Components. *J. Power Sources* **1992**, *39* (1), 21–41.

(21) Li, Q.; Peng, H.; Wang, Y.; Xiao, L.; Lu, J.; Zhuang, L. The Comparability of Pt to Pt-Ru

in Catalyzing the Hydrogen Oxidation Reaction for Alkaline Polymer Electrolyte Fuel Cells Operated at 80 °C. *Angew. Chemie - Int. Ed.* **2019**, *58* (5), 1442–1446.

(22) Bellini, M.; Pagliaro, M. V.; Lenarda, A.; Fornasiero, P.; Marelli, M.; Evangelisti, C.; Innocenti, M.; Jia, Q.; Mukerjee, S.; Jankovic, J.; Wang, L.; Varcoe, J. R.; Krishnamurthy, C. B.; Grinberg, I.; Davydova, E.; Dekel, D. R.; Miller, H. A.; Vizza, F. Palladium-Ceria Catalysts with Enhanced Alkaline Hydrogen Oxidation Activity for Anion Exchange Membrane Fuel Cells. *ACS Appl. Energy Mater.* **2019**, *2* (7), 4999–5008.

(23) Sankar, S.; Anilkumar, G. M.; Tamaki, T.; Yamaguchi, T. Binary Pd−Ni Nanoalloy Particles over Carbon Support with Superior Alkaline Formate Fuel Electrooxidation Performance. *ChemCatChem* **2019**, *11* (19), 4731–4737.

(24) Zhao, Y.; Wang, G.; Xiao, L.; Lu, J.; Zhuang, L. Hydrogen Oxidation Reaction on Pd-Ni(OH)2 Composite Electrocatalysts in an Alkaline Electrolyte. *ChemistrySelect* **2020**, *5* (26), 7803–7807.

(25) Kiros, Y.; Schwartz, S. Long-Term Hydrogen Oxidation Catalysts in Alkaline Fuel Cells. *J. Power Sources* **2000**, *87* (1), 101–105.

(26) N. Borchtchoukova, V. Feldman, G. Finkelshtain, S.K. Rakovsky, M.V. Gabrovska, D.A. Nikolova, L.P. Bilyarska, Nickel-based catalysts for fuel cells, US 10,522,844 B2, Gencell Ltd., Petah Tikva (IL), Israel, 2019, p. 14.

(27) G. Finkelshtain, K. Petrov, Nino, N. Borchtchoukova, Y. Pashkevich, Gas diffusion electrode and process for making same, US 9 , 966 , 609 B2, GenCell LTD ., Petah Tikva (IL), Israel, 2018.

(28) Miller, H. A.; Vizza, F.; Marelli, M.; Zadick, A.; Dubau, L.; Chatenet, M.; Geiger, S.;

Cherevko, S.; Doan, H.; Pavlicek, R. K.; Mukerjee, S.; Dekel, D. R. Highly Active Nanostructured Palladium-Ceria Electrocatalysts for the Hydrogen Oxidation Reaction in Alkaline Medium. *Nano Energy* **2017**, *33* (November 2016), 293–305.

(29) Alinejad, S.; Quinson, J.; Schröder, J.; Kirkensgaard, J. J. K.; Arenz, M. Carbon-Supported Platinum Electrocatalysts Probed in a Gas Diffusion Setup with Alkaline Environment: How Particle Size and Mesoscopic Environment Influence the Degradation Mechanism. *ACS Catal.* **2020**, *10* (21), 13040–13049.

(30) Kabir, S.; Zadick, A.; Atanassov, P.; Dubau, L.; Chatenet, M. Stability of Carbon-Supported Palladium Nanoparticles in Alkaline Media: A Case Study of Graphitized and More Amorphous Supports. *Electrochem. commun.* **2017**, *78*, 33–37. https://doi.org/10.1016/j.elecom.2017.03.017.

(31) Castanheira, L.; Dubau, L.; Mermoux, M.; Berthomé, G.; Caqué, N.; Rossinot, E.; Chatenet, M.; Maillard, F. Carbon Corrosion in Proton-Exchange Membrane Fuel Cells: From Model Experiments to Real-Life Operation in Membrane Electrode Assemblies. *ACS Catal.* **2014**, *4* (7), 2258–2267.

(32) Castanheira, L.; Silva, W. O.; Lima, F. H. B.; Crisci, A.; Dubau, L.; Maillard, F. Carbon Corrosion in Proton-Exchange Membrane Fuel Cells: Effect of the Carbon Structure, the Degradation Protocol, and the Gas Atmosphere. *ACS Catal.* **2015**, *5* (4), 2184–2194.

(33) G. Jerkiewicz. Hydrogen Sorption at/in Electrodes. *Science (80-.).* **1998**, *57* (2), 137–186.

(34) Rand, D. A. J.; Woods, R. The Nature of Adsorbed Oxygen on Rhodium, Palladium and Gold Electrodes. *J. Electroanal. Chem.* **1971**, *31* (1), 29–38.

(35) T. Chierchie, C. Mayer, W. J. L. Structural Changes of Surface Oxide Layers on

Palladium. *J. Electroanal. Chem. Interfacial Electrochem.* **1982**, *135*, 211–220.

(36) Miller, H. A.; Lavacchi, A.; Vizza, F.; Marelli, M.; Di Benedetto, F.; D'Acapito, F.; Paska, Y.; Page, M.; Dekel, D. R. A Pd/C-CeO2Anode Catalyst for High-Performance Platinum-Free Anion Exchange Membrane Fuel Cells. *Angew. Chemie - Int. Ed.* **2016**, *55* (20), 6004–6007.

(37) Zheng, J.; Zhou, S.; Gu, S.; Xu, B.; Yan, Y. Size-Dependent Hydrogen Oxidation and Evolution Activities on Supported Palladium Nanoparticles in Acid and Base. *J. Electrochem. Soc.* **2016**, *163* (6), F499–F506.

(38) Jiang, L.; Hsu, A.; Chu, D.; Chen, R. Size-Dependent Activity of Palladium Nanoparticles for Oxygen Electroreduction in Alkaline Solutions. *J. Electrochem. Soc.* **2009**, *156* (5), B643.

(39) Mansor, M.; Timmiati, S. N.; Wong, W. Y.; Zainoodin, A. M.; Lim, K. L.; Kamarudin, S. K. Nipd Supported on Mesostructured Silica Nanoparticle as Efficient Anode Electrocatalyst for Methanol Electrooxidation in Alkaline Media. *Catalysts* **2020**, *10* (11), 1–20.

(40) Xie, L.; Kirk, D. W. Nickel Catalyst Migration in an Anion Exchange Membrane Fuel Cell. *Electrochim. Acta* **2020**, *364*, 137091.

(41) Belenov, S. V; Guterman, V. E.; Popov, L. D.; Kozakov, A. T.; Nikolsky, A. V; Danilenko, M. V; Safronenko, O. I.; Nikulin, A. Y. The Study of the Pyrolysis Products of Ni (II) and Pd (II) Chelate Complexes as Catalysts for the Oxygen Electroreduction Reaction. *J. Solid State Electrochem.* **2020**.